Angewandte Chemie International Edition

Angewandte International Edition Chemie

GDCh German Chemical Society

How to cite: *Angew. Chem. Int. Ed.* **2026**, e21015
doi.org/10.1002/anie.202521015

RESEARCH ARTICLE Hot Paper

Correlating Structure Change With Magnetic Ordering and Spin Fluctuation During Delithiation of Transition Metal Layered Oxide

Mingjian Zhang[1,2] | Zhefeng Chen[3] | Tongchao Liu[4] | Deshun Hong[5] | Longlong Fan[6] | Ziyan Wu[1] | Yang Ren[7] | Yu-Sheng Chen[8] | Feng Pan[3]

[1]School of Science and Engineering, The Chinese University of Hong Kong, Shenzhen, China | [2]Guangdong Basic Research Center of Excellence for Aggregate Science, School of Science and Engineering, The Chinese University of Hong Kong Shenzhen, Shenzhen, Guangdong, China | [3]School of Advanced Materials, Peking University, Graduate School Shenzhen, Shenzhen, China | [4]Chemical Sciences and Engineering Division, Argonne National Laboratory, Lemont, Illinois, USA | [5]Department of Applied Physics, and Center of Quantum Materials and Devices, Chongqing University, Chongqing, China | [6]Beijing Synchrotron Radiation Facility, Institute of High Energy Physics, Chinese Academy of Sciences, Beijing, China | [7]Department of Physics, JC STEM Lab of Energy and Materials Physics, and Shenzhen Research Institute, City University of Hong Kong, Hong Kong, China | [8]ChemMatCARS, the University of Chicago, Lemont, Illinois, USA

Correspondence: Mingjian Zhang (zhangmingjian@cuhk.edu.cn) | Yang Ren (yangren@cityu.edu.hk) | Yu-Sheng Chen (yushengchen@uchicago.edu) | Feng Pan (panfeng@pkusz.edu.cn)

Received: 24 September 2025 | **Revised:** 26 January 2026 | **Accepted:** 27 January 2026

Keywords: delithiation | $LiCoO_2$ | magnetic ordering | spin fluctuation | structure change

ABSTRACT

Current Li-ion battery technology relies on Li^+ insertion/extraction coupled with electron gaining/loss at both cathodes and anodes. Although extensive efforts have been devoted to studying the structure change of cathode materials with Li^+ extraction/insertion, changes in the magnetic properties arising from the accompanying redox processes have been largely overlooked. Here, we systematically investigate both the structure evolution and magnetic-property changes during the delithiation of the representative layered oxide $LiCoO_2$, by combining the operando synchrotron-based x-ray diffraction with dedicated magnetic measurements. We construct a magnetic phase diagram as a function of Li content x in Li_xCoO_2, which closely mirrors the corresponding structure evolution diagram. The results reveal a series of complicated magnetic transitions upon Li extraction: paramagnetic → antiferromagnetic → paramagnetic → diamagnetic → paramagnetic. Moreover, the variation in the effective magnetic moment of Co^{4+} is strongly correlated with local structural changes within the CoO_6 octahedra, indicating that the Co^{4+} spin-state fluctuation may play an important role in the structure evolution and electrochemical performance. These findings help close a critical gap in understanding structure-magnetism coupling during the electrochemical cycling and may inspire the design of new layered oxide cathodes from a spin-electronics perspective.

1 | Introduction

Metal oxides represent one of the most important classes of functional materials due to their natural abundance and diverse structures, which enable applications spanning optics, electronics, magnetism, catalysis, and energy conversion/storage [1–4]. Among them, lithium transition metal (TM = Ni, Co, Mn) layered oxides have emerged as a prominent cathode material

M. Zhang and Z. Chen contributed equally to this study.

family for Li-ion batteries (LIBs) since the pioneering discovery of $LiCoO_2$ in the 1980s, owing to their excellent electrochemical performance [5–8]. Recent advances, particularly the gradient disordering strategy, have pushed the practical capacity of $LiCoO_2$ toward its theoretical limit [9], underscoring the critical role of understanding structural stability during electrochemical cycling [10].

The structure evolution of TM layered oxides during the charge/discharge (Li^+ insertion/extraction) has been extensively studied. Taking $LiCoO_2$ as a representative, the phase transition diagram as a function of Li content x in Li_xCoO_2 was established in the 1990s [11–15]. The process involves five phase transitions and six distinct phases: (1) transformation from the initial hexagonal phase (H1) to a second hexagonal phase (H2), with an intervening two-phase coexistence region; (2) rapid transition from H2 to a monoclinic phase (M1); (3) existence of M1 phase within a narrow composition range ($x \approx 0.05$), followed by swift transformation to a third hexagonal phase (H3); (4) transition from H3 to a second monoclinic phase (M2), again accompanied by two-phase coexistence; and (5) final transformation of M2 to O1 phase upon complete Li^+ extraction. The three hexagonal phases (H1, H2, and H3) share the same space group (*R*-3*m*), and M1 phase belongs to *C*2/*c*, and O1 phase was assigned to *P*-3*m*1 by Tarascon group [12]. While the M2 phase remains experimentally uncharacterized, its structure has been theoretically predicted by the Ceder group [13, 16]. Although the phase evolution sequence is well-documented, the fundamental mechanisms driving these phase transitions, especially their relationship with Li content *x*, remain elusive.

From an electrochemical perspective, the charge/discharge process involves not only Li^+ insertion/extraction but also TM redox reactions. Changes in TM valence states, resulting from the electron loss/gain, can significantly influence the spin configuration of *d*-electrons and consequently affect the magnetic and electronic properties of the material. Previous studies have shown that the H1 → H2 phase transition in Li_xCoO_2 coincides with a semiconductor-to-metal transition, a high-spin state has been identified at $x = 0.94$. [17] Magnetic properties of Li_xCoO_2 have also been reported to vary with Li content. [18–20] Furthermore, correlations between magnetic behavior and electrochemical performance have been established in other cathode systems, including magnetic frustration in Ni—Co—Mn ternary layered oxides, [21] and spin fluctuations in $LiFePO_4$. [22] These observations suggest that structural phase transition may be more intimately connected with the redox-induced magnetic evolution than previously recognized–a relationship that remains largely unexplored.

To elucidate the connection between structure changes and magnetic properties, we combined operando synchrotron-based x-ray diffraction with precise magnetic measurements to study the structural and magnetic evolution of $LiCoO_2$ during electrochemical cycling. We established comprehensive diagrams of both phase evolution and magnetic behavior as functions of Li content, revealing a one-to-one correspondence among them. The underlying spin fluctuations were identified and explained through crystal field theory, highlighting the role of local structural changes within TMO_6 octahedra. These findings provide new magnetic insights into TM oxide systems and offer guidance for designing advanced layered oxide cathodes for high-performance energy storage applications.

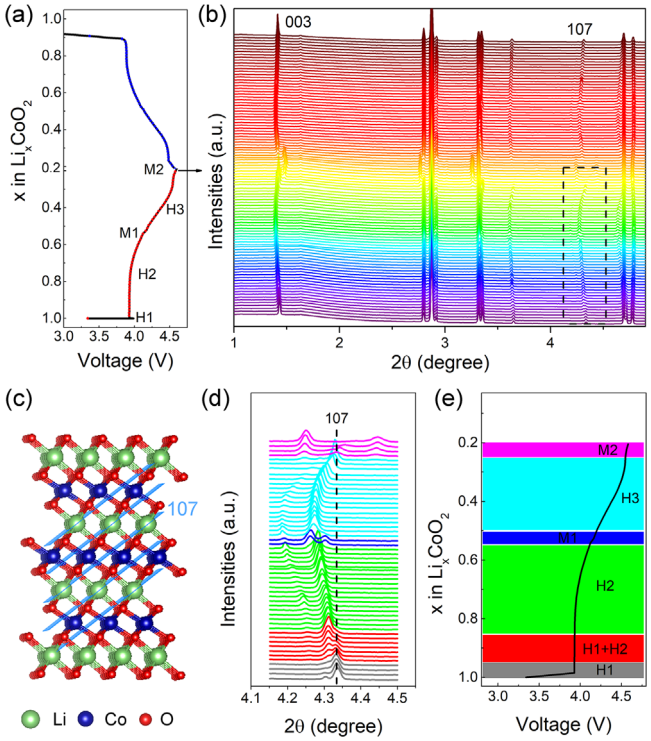

FIGURE 1 | Structural change of $LiCoO_2$ under the upper cutoff voltage 4.6 V. (a) The first charge/discharge curve of $LiCoO_2$ monitoring by the real-time HEXRD technique. The wavelength is 0.1173 Å. (b) In situ XRD patterns recorded during the first charge/discharge of $LiCoO_2$. (c) The structure diagram of $LiCoO_2$ with 107 crystallographic plane marked by the blue planes. (d) The peak evolution around 107 characteristic peak during the first charge, enlarged from the region marked by the blue dashed square in (b), to distinguish the detailed phase evolution. (e) The phase evolution as a function of Li content x in Li_xCoO_2, deduced from the peak evolution of 107 characteristic peak in (d).

2 | Results and Discussion

The structural changes in Li_xCoO_2 during the charge/discharge below 4.3 V (corresponding to $1>x>0.5$), have been extensively documented, revealing a two-step phase change from the initial layered H1 phase to H2, and subsequently to the monoclinic M1 phase. [11–15] To complement previous findings, we employed operando high-energy x-ray diffraction (HEXRD) to re-examine this process. Figure 1a, b presents the first charge/discharge profile of $LiCoO_2$ as well as the corresponding HEXRD patterns. Two distinct groups of diffraction peaks exhibit opposite shifting trends (Figure S1): Group I peaks (003, 104, 015, 107, and 018) initially shift to low angles before moving to higher angles, while Group II peaks (101, 110) display the reverse behavior. Since Group I peaks primarily reflect the interlayer spacing along the *c*-axis, while Group II peaks correspond to in-plane *a*/*b*-axis parameters. These opposing trends suggest that interlayer and intralayer structural changes occur in a compensatory manner during cycling, likely driven by Co redox reactions and associated electrostatic interactions.

Given the structural similarity among H1, H2, and M1 phases, distinguishing phase transitions using conventional peaks (e.g., 003, 104) proves challenging. We therefore selected the 107 peak (originating from the high-index crystallographic planes involving Li ions) as a sensetive indicator of the phase transition, due to its high angular resolution and the prounced response to Li^+ extraction (Figure 1c). Figure 1d tracks the 107 peak during charging, clearly revealing four phase transtions involving five distinct phases below 4.6 V: H1 → H2 → M1 → H3 → M2. The process can be divided to six regions based on phase coexistence: (I) pure H1 phase with constant peak position of 107 peak; (II) H1+H2 coexsitence region with invariant peak positions but changing phase fractions (Figure S2), hinting a first-order phase transition; (III) pure H2 phase; (IV) pure M1 phase; (V) pure H3 phase; and (VI) M2 phase. As summarized in Figure 1e, these regions correlate with specific Li content ranges: H1 (x = 1–0.85), H2 (x = 0.95–0.55), M1 (x = 0.55–0.50), H3 (x = 0.50–0.25), and M2 (x < 0.25).

To investigate the magnetic behaviors during delithiation, we prepared Li_xCoO_2 samples across the entire composition range (x = 0.97, 0.75, 0.65, 0.56, 0.53, 0.5, 0.44, 0.39, 0.33, and 0.2) via electrochemical methods (Figure S3). Magnetization-temperature (M-T) measurements (Figure 2a) reveal three distinct magnetic behaviors:. MB1 (paramagnetic) for x = 0.97 and 0.75,; MB2 (paramagnetic→ antiferromagnetic→ paramagnetic) for 0.65 ≥ x ≥ 0.44), characterized by a Néel temperature (T_N) around 160 K (Figure 2a inset, Figure S4); [18–20] and MB3 (diamagnetic→paramagnetic) for $x \leq 0.39$. The antiferromagnetic transition intensity in MB2 samples increases with decreasing x from 0.65 to 0.44, suggesting phase-composition dependence. The magnetic property of $LiCoO_2$ after long-term cycling was also studied (Figure S5), revealing a paramagnetic behavior with larger magnetization.

Figure 2b correlates magnetic behavior with phase composition as functions of Li content x. MB1 corresponds to H1/H2 phases (dominated by H1), MB2 associates with H2/M1/H3 phases (strongly linked to M1, given the pronounced antiferromagnetism at x = 0.5)., while MB3 relates to H3/M2 phases (diamagnetic character weakening upon transiotn to M2 phase at x = 0.2). Ex situ XRD patterns of cycled samples (Figure S6) confirms these assignments: H1 phase dominates at x = 0.97 and 0.75 (MB1); H2 phase at x = 0.65-0.53 and M1 at x = 0.5–0.44 (MB2); and H3 phase at. x = 0.39–0.20 (MB3). The diamagnetic response in MB3 suggests absence of unpaired electrons, hinting at the possible existence of Co^{5+} ($3d^4$ with low-spin configuration). [23, 24]

The magnetic properties of $LiCoO_2$ stem from the $Co^{3+/4+}$ electronic configurations. While Co^{3+} ($3d^6$) adopts a low-spin state with no unpaired electrons, Co^{4+} ($3d^5$) exhibits variable spin states depending on crystal field conditions (Figure 3a). All the Co cations locate at the octahedral sites, coordinated with six oxygen anions, and the spin state is determined by the configuration of the CoO_6 octahedron, including Co—O bond lengths and O-Co-O bond angles. As shown in the right panel of Figure 3a, there are two kinds of spin states, low-spin and high-spin. Based on the crystal field theory (CFT), (25) when the crystal field is strong, orbital splitting energy (Δ) between e_g and t_{2g} is larger than electron pairing energy (P), leading to a low-spin configuration

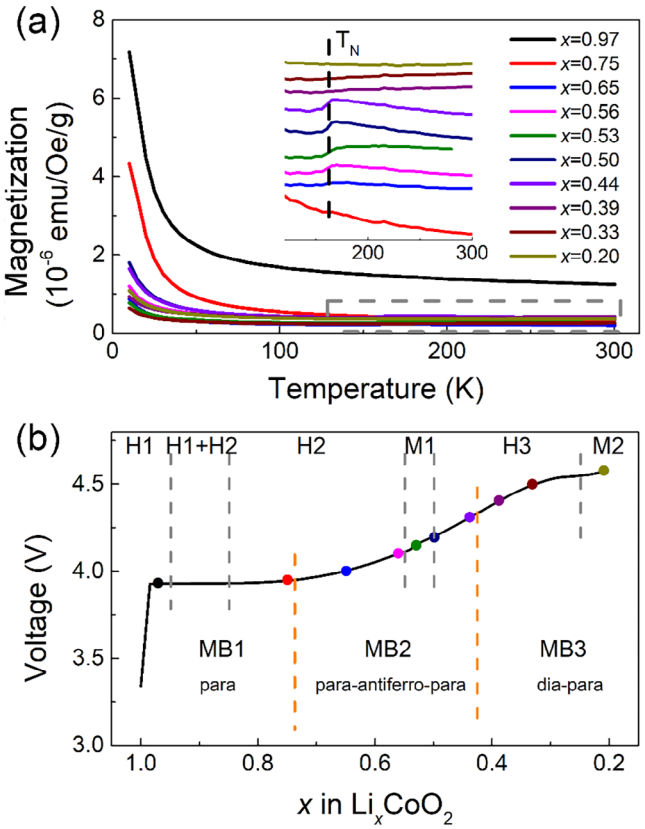

FIGURE 2 | The evolution of magnetic behaviors during delithiation of $LiCoO_2$. (a) The M-T curves of ten Li_xCoO_2 samples (x = 0.97, 0.75, 0.65, 0.56, 0.53, 0.5, 0.44, 0.39, 0.33 and 0.2). The inset is enlarged from the region marked by the dashed rectangle, to show the variation of M values at high temperatures (120-300 K). (b) The magnetic behaviors (MB) and phase compositions as a function of Li content x in Li_xCoO_2. The magnetic behaviors are divided into 3 kinds: (1) MB1: paramagnetic (para); (2) MB2: paramagnetic evolves to antiferromagnetic, then to paramagnetic with temperature (para-antiferro-para); (3) MB3: diamagnetic evolves to paramagnetic (dia-para).

of $t_{2g}^5e_g^0$ with one unpaired electron. The high-spin configuration of $t_{2g}^3eg^2$ with 5 unpaired electrons is induced by the weak crystal field ($\Delta < P$). The magnetic moments are estimated as 1.73 and 5.92 μ_B for each low-spin and high-spin Co^{4+} cation, respectively, according to the formula $\sqrt{n(n+2)}$ (n is the number of unpaired electrons).

To get insight into the variation of the spin state of Co^{4+} during delithiation of $LiCoO_2$, the magnetic fitting was performed on the M-T curves of the ex situ samples above using the Curie-Weiss law $\chi_m = \frac{C}{T-\theta} + \chi_0$.(26–28) Temperature-independent magnetic susceptibility χ_0, the Curie constant C and the Weiss temperature θ are plotted as a function of Li content x (Figure S7). Furthermore, the effective magnetic moment μ_{eff} for each Co^{4+} cation is deduced from the Curie constant C (Figure S8). As shown in Figure 3b, μ_{eff} is 4.16 μ_B per Co^{4+} when x = 0.97, approaching the limit for high-spin Co^{4+} (the upper horizontal red line). It indicates predominantly high-spin Co^{4+} during the early stage of delithitation. With the decrease of Li content x, μ_{eff} fast decays lower than 1.73 μ_B for the low-spin Co^{4+} (the lower horizontal red line), signaling spin-state transition from high-spin to low-spin Co^{4+}. This spin reconfiguration from high-spin to low-spin

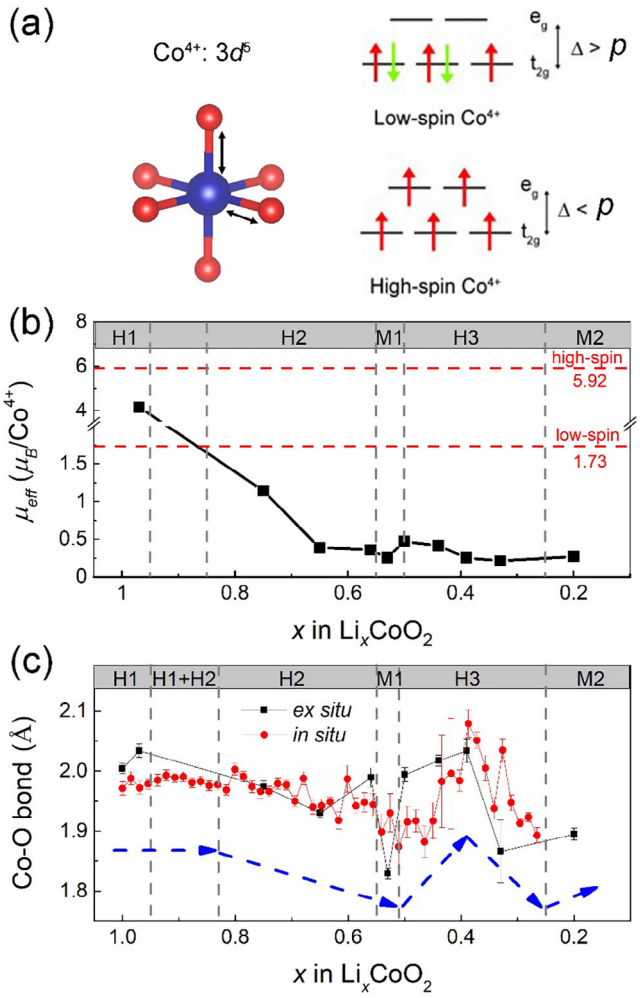

FIGURE 3 | The change in the spin state of Co cations during delithiation of $LiCoO_2$. (a) The structure of $Co^{4+}O_6$ octahedron and the analysis of low-spin and high-spin states for Co^{4+} using the crystal field theory. The orbital splitting energy and the electron pairing energy are denoted as Δ and *P*, respectively. (b) The effective magnetic moment μ_{eff} of Co^{4+} as a function of Li content x in Li_xCoO_2. The theoretical μ_{eff} values for high-spin and low-spin Co^{4+} are labeled by two dashed horizontal lines. (c) The Co—O bond length as a function of Li content x in Li_xCoO_2. The Co—O bond lengths were deduced from the Rietveld refinement of in situ and ex situ XRD patterns with charging. The dashed blue arrows are used to guide the eye in showing the variation trends in different phase regions.

accompanies with the phase transition from the H1 phase to the H2 and M1 phases. When $x = 0.5$, there is a little jump in the μ_{eff} value, corresponding to the phase transition from M1 phase to H3 phase. When *x* decreases from 0.5 to 0.33, μ_{eff} gradually decreases. Eventually, a little lift in the μ_{eff} value is observed at $x = 0.2$.

As we discussed above, the variation of spin state for Co^{4+} should be closely related to the change in the crystal field of CoO_6 octahedron, which is determined by the coordination configuration of CoO_6 octahedron, involving changes in Co—O bond length and O—Co—O bond angle. Rietveld refinement was performed on operando and ex situ XRD patterns to deduce the bond lengths of Li—O and Co—O and the bond angles of O—Li—O and O—Co-O (Figure S9). As shown in Figure 3c, Co—O bond

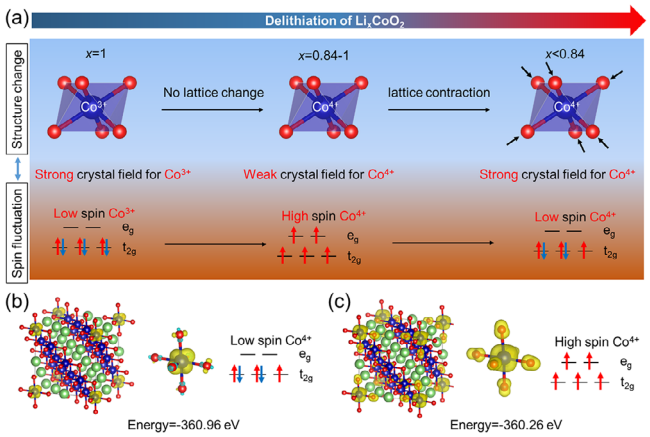

FIGURE 4 | Correlating the structural change with the spinel fluctuation during deliathiation. (a) Schematic illustration of the relationship between the local structural change in CoO_6 octahedron and the spin fluctuation of Co cations. (b, c) The structure of $Li_{0.9375}CoO_2$ (Color code: Co, blue; Li, green; O, red) and the magnetization density distribution maps for the low-spin and high-spin $Co^{4+}O_6$ octahedron. Yellow and turquoise isosurfaces denote areas of positive and negative values (±0.01 e $bohr^{-3}$), respectively.

length is plotted as a function of Li content x. It varies little in H1 and H1+H2 regions, then gradually decreases in the region of the H2 phase, and reaches its minimum in the M1 region. In the H3 region, it first goes upward and then downward. The variation trend of the Co—O bond length is guided by the dashed blue arrows, showing a similar change trend to that of μ_{eff} in Figure 3b. In addition, the variations of TM-slab and O—Co—O bond angle also demonstrate a similar trend (Figure S9c–f). Therefore, we can deduce that the variation of spin state does not have one-to-one correspondence relation with the change in different phase structures, while is closely correlated with the local structure change within the CoO_6 octahedron.

Since the structural change in the CoO_6 octahedron is found highly related to the spin state change of Co cation, we propose a CFT-based mechanism to explain the spin fluctuations (Figure 4a). In pristine $LiCoO_2$ ($x = 1$), Co^{3+} is located at the central position of CoO_6 octahedron, keeping the electrostatic force balance in the initial structure. Therefore the strong crystal field exists, leading to a larger orbit-splitting energy between e_g and t_{2g} than the electron pairing energy ($\Delta > P$), yielding a low-spin state for Co^{3+}. In the early stage of charge (x = 1–0.84), a small amount of Co^{3+} (<16%) is oxidized to Co^{4+} while no structure variation occurs within CoO_6 octahedron, namely no change in Co—O bond length and O—Co—O bond angle (Figure S9). Therefore, the strong crystal field for Co^{3+} transforms to a weak crystal field for Co^{4+}, resulting into a smaller orbit splitting energy between e_g and t_{2g} than the electron pairing energy ($\Delta < P$), thus a high-spin state for Co^{4+}. This is the fundamental structural origin for the spin fluctuation from low-spin Co^{3+} to high-spin Co^{4+}. As delithiation proceeds ($x < 0.84$), the decrease in Co—O bond length (Figure 3c) indicates the contraction of $Co^{4+}O_6$ octahedron, making the weak crystal field evolve into the strong crystal field for Co^{4+}. Correspondingly, the high-spin state gradually changes back to the low-spin state. In brief, the spin fluctuation of Co^{4+} arises from the intensity variation of the

crystal field, resulting from the local structure changes within CoO_6 octahedron, which are greatly associated with the phase transition.

To further validate the hypothesis, the density functional theory (DFT) calculations were performed based on a slightly delithiated structural model $Li_{0.9375}CoO_2$ with low-spin Co^{4+} and high-spin Co^{4+} (Figure S10), respectively. The magnetization density distribution was plotted in Figures 4b, c. First, the total energy of the low-spin system (−360.96 eV) is lower than that of the high-spin system (−360.26 eV), confirming that the high-spin state is thermodynamically metastable. It explains the spin transformation of Co^{4+} from the high-spin state to the low-spin state with further delithiation above. In addition, the magnetization density distribution map of the low-spin $Co^{4+}O$ (16) octahedron (the right panel of Figure 4b) exhibits the concentrated spin electrons at the center Co^{4+} cation, hinting at the weak electronic interaction between the center Co^{4+} cation and six coordinated O anions. Differently, the spin electrons locate at both the center Co^{4+} cation and six coordinated O anions in the magnetization density distribution map of high-spin $Co^{4+}O$ (16) octahedron (the right panel of Figure 4c), indicating the strong electronic interaction between the center Co^{4+} cation and six coordinated O anions. The significant difference in electronic structure may provide the driving force for the contraction of the CoO_6 octahedron and the macroscopic phase transitions.

To further examine the dependence of Co spin state on the delithiation extent, we performed DFT calculations using the structure models of Li_xCoO_2 with different delithiation extents (x = 0.9375, 0.875, 0.75 and 0.5). As shown in Figure S11 and Table S1, the structures with low-spin Co^{4+} always have the lower system energies than the corresponding structures with high-spin Co^{4+}. The results indicate that the structures with low-spin Co^{4+} are more stable than those with high-spin Co^{4+}. The structures with high-spin Co^{4+} are actually metastable because the structure changes with delithiation lag behind the changes in the oxidation state of Co cation. This "lag" between redox and structural response provides a novel thermodynamic perspective on the phase transition energy landscape in layered oxides.

3 | Conclusion

In summary, we have thoroughly elucidated the evoluiton of magnetic behaviors and spin states of metal cations during the electrochemical delithiation of the representative cathode $LiCoO_2$. Our study reveals a complex sequence of magnetic transitions—transitioning from paramagnetic to antiferromagnetic, then back to paramagnetic, followed by a diamagnetic regime, and finally returning to a paramagnetic state. Accompanying with these transitions, the effective magnetic moment μ_{eff} of Co^{4+} cation exhibits a large value (>4 μ_B) in the early delitiation stage (x = 1–0.84), followed by a rapid decline to approximately 0.5 μ_B at higher states of charge. This shift signifies a spin-state transition of Co^{4+} from a high-spin to a low-spin configuration. By integrating Crystal Field Theory (CFT) with DFT calculations, we establish for the first time a fundamental link between these spin-state fluctuations and the local structural distortions within the CoO_6 octahedra. These findings demonstrate that magnetic properties are intrinsic indicators of structural evolution in battery cathodes. Our work not only bridges the gap between electrochemistry and magnetism but also provides a new conceptual framework—spin-state engineering—for the design and optimization of high-performance layered oxide materials for next-generation energy storage.

Acknowledgments

This work is supported by the National Natural Science Foundation of China (52172175), the Program from Guangdong Introducing Innovative and Entrepreneurial Teams (2019ZT08L101 and RCTDPT-2020-001), Guangdong Basic Research Center of Excellence for Aggregate Science, 1+1+1 CUHK-CUHK(SZ)-GDSTC Joint Collaboration Fund (2025A0505000048), the Shenzhen Science and Technology Research Program (JCYJ20250604141048025, and JCYJ20220818101016034), the Hong Kong Research Grants Council (9043699). NSF's ChemMatCARS, Sector 15 at the Advanced Photon Source (APS), Argonne National Laboratory (ANL) is supported by the Divisions of Chemistry (CHE) and Materials Research (DMR), National Science Foundation, under grant number NSF/CHE-2335833.Y.R. would like to express the sincere appreciation to the Hong Kong SAR government for supporting the research under the Global STEM Professorship, and to the Hong Kong Jockey Club for supporting the research under the JC STEM Lab of Energy and Materials Physics. This research used resources of the Advanced Photon Source, a U.S. Department of Energy (DOE) Office of Science user facility operated for the DOE Office of Science by Argonne National Laboratory under Contract No. DE-AC02-06CH11357.

Conflicts of Interest

The authors declare no conflicts of interest.

Data Availability Statement

The data that support the findings of this study are available in the Supporting Information of this article.

References

1. S. S. Cheema, N. Shanker, L. C. Wang, et al., "Ultrathin Ferroic HfO_2–ZrO_2 Superlattice Gate Stack for Advanced Transistors," *Nature* 604 (2022): 65–71, https://doi.org/10.1038/s41586-022-04425-6.

2. X. W. Xie, Y. Li, Z. Q. Liu, M. Haruta, and W. J. Shen, "Low-Temperature Oxidation of CO Catalysed by Co_3O_4 Nanorods," *Nature* 458 (2009): 746–749, https://doi.org/10.1038/nature07877.

3. Y. Y. Wang, N. S. Rogado, R. J. Cava, and N. P. Ong, "Spin Entropy as the Likely Source of Enhanced Thermopower in $Na_xCo_2O_4$," *Nature* 423 (2003): 425–428, https://doi.org/10.1038/nature01639.

4. N. P. Lu, P. F. Zhang, Q. H. Zhang, et al., "Electric-Field Control of Tri-State Phase Transformation With a Selective Dual-Ion Switch," *Nature* 546 (2017): 124–128, https://doi.org/10.1038/nature22389.

5. Q. Liu, X. Su, D. Lei, et al., "Approaching the Capacity Limit of Lithium Cobalt Oxide in Lithium Ion Batteries via Lanthanum and Aluminium Doping," *Nature Energy* 3 (2018): 936–943, https://doi.org/10.1038/s41560-018-0180-6.

6. K. Mizushima, P. C. Jones, P. J. Wiseman, and J. B. Goodenough, "Li_xCoO_2 (0<x<-1): A New Cathode Material for Batteries of High Energy Density," *Materials Research Bulletin* 15 (1980): 783–789, https://doi.org/10.1016/0025-5408(80)90012-4.

7. Y. Shao-Horn, L. Croguennec, C. Delmas, E. C. Nelson, and M. A. O'Keefe, "Atomic Resolution of Lithium Ions in $LiCoO_2$," *Nature Materials* 2 (2003): 464–467, https://doi.org/10.1038/nmat922.

8. J. N. Zhang, Q. H. Li, C. Y. Ouyang, et al., "Trace Doping of Multiple Elements Enables Stable Battery Cycling of $LiCoO_2$ at 4.6 V," *Nature Energy* 4 (2019): 594–603, https://doi.org/10.1038/s41560-019-0409-z.

9. W. Y. Huang, J. Y. Li, Q. H. Zhao, et al., "Mechanochemically Robust $LiCoO_2$ With Ultrahigh Capacity and Prolonged Cyclability," *Advanced Materials* 36 (2024): 2405519, https://doi.org/10.1002/adma.202405519.

10. J. Y. Li, C. Lin, M. Y. Weng, et al., "Structural Origin of the High-Voltage Instability of Lithium Cobalt Oxide," *Nature Nanotechnology* 16 (2021): 599–605, https://doi.org/10.1038/s41565-021-00855-x.

11. T. Ohzuku, A. Ueda, "Solid-State Redox Reactions of $LiCoO_2$ (R3m) for 4 Volt Secondary Lithium Cells," *Journal of the Electrochemical Society* 141 (1994): 2972–2977, https://doi.org/10.1149/1.2059267.

12. G. G. Amatucci, J. M. Tarascon, L. C. Klein, "CoO_2, The End Member of the Li X CoO_2 Solid Solution," *Journal of the Electrochemical Society* 143 (1996): 1114–1123, https://doi.org/10.1149/1.1836594.

13. A. Van der Ven, M. K. Aydinol, G. Ceder, "First-Principles Evidence for Stage Ordering in Li_xCoO_2,"*Journal of the Electrochemical Society* 145 (1998): 2149–2155.

14. J. N. Reimers, J. R. Dahn, "Electrochemical and in Situ X-Ray Diffraction Studies of Lithium Intercalation in Li_XCoO_2," *Journal of the Electrochemical Society* 139 (1992): 2091–2097, https://doi.org/10.1149/1.2221184.

15. A. Van der Ven, M. K. Aydinol, G. Ceder, G. Kresse, and J. Hafner, "First-principles Investigation of Phase Stability in Li_xCoO_2," *Physical Review B* 58 (1998): 2975–2987, https://doi.org/10.1103/PhysRevB.58.2975.

16. D. Carlier, A. Van der Ven, C. Delmas, and G. Ceder, "First-Principles Investigation of Phase Stability in the O_2-$LiCoO_2$ System," *Chem. Mater.* 15 (2003): 2651–2660, https://doi.org/10.1021/cm030002t.

17. J. T. Hertz, Q. Huang, T. McQueen, et al., "Magnetism and Structure of Li_xCoO_2 and Comparison to Na_xCoO_2," *Physical Review B* 77 (2008): 075119, https://doi.org/10.1103/PhysRevB.77.075119.

18. K. Miyoshi, C. Iwai, H. Kondo, M. Miura, S. Nishigori, and J. Takeuchi, "Magnetic and Electronic Properties of Li_xCoO_2 Single Crystals," *Physical Review B* 82 (2010): 075113, https://doi.org/10.1103/PhysRevB.82.075113.

19. K. Mukai, Y. Ikedo, H. Nozaki, et al., "Magnetic Phase Diagram of Layered Cobalt Dioxide Li_xCoO_2," *Physical Review Letter* 99 (2007): 087601, https://doi.org/10.1103/PhysRevLett.99.087601.

20. K. Miyoshi, H. Kondo, M. Miura, C. Iwai, K. Fujiwara, and J. Takeuchi, "Magnetic and Transport Properties of Layered Li_xCoO_2 Single Crystals," *Journal of Physics: Conference Series* 150 (2009): 042129.

21. J. X. Zheng, Y. K. Ye, T. C. Liu, et al., "Ni/Li Disordering in Layered Transition Metal Oxide: Electrochemical Impact, Origin, and Control," *Accounts of Chemical Research* 52 (2019): 2201–2209, https://doi.org/10.1021/acs.accounts.9b00033.

22. J. Hu, H. Zeng, X. Chen, et al., "Revealing Insights Into Li_XFePO_4 Nanocrystals With Magnetic Order at Room Temperature Resulting in Trapping of Li Ions," *Journal of Physical Chemistry Letters* 10 (2019): 4794–4799, https://doi.org/10.1021/acs.jpclett.9b01557.

23. S. Landron and M. B. Lepetit, "*Ab Initio* Evaluation of the Local Effective Interactions in the Superconducting Compound $Na_{0.35}$ Co O_2 • $1.3H_2O$," *Physical Review B* 74 (2006): 184507.

24. V. I. Dimza, "EPR Studies of Mn, Fe, Co, and Cu Doped PLZT and PMN Compositions," *Phys Stat Sol (a)* 140 (1993): 543–551.

25. H. A. Bethe, "Termaufspaltung in Kristallen," *Annalen Der Physik* 395 (1929): 133–208, https://doi.org/10.1002/andp.19293950202.

26. S. Blundell, *Magnetism in Condensed Matter* (Oxford University Press: 2001), https://doi.org/10.1093/oso/9780198505921.001.0001.

27. N. A. Spaldin, *Magnetic Materials: Fundamentals and Applications* (Cambridge University Press, 2010), https://doi.org/10.1017/CBO9780511781599.

28. J. M. Coey, *Magnetism and Magnetic Materials* (Cambridge University Press, 2010).

Supporting Information

Additional supporting information can be found online in the Supporting Information section.

Supporting File 1: anie71380-sup-0001-SuppMat.docx.